Spectroscopic and Structural Characterization of Low-Level Alkali Doping Effects on Mo/Silica−Titania Catalysts

Rick B. Watson and Umit S. Ozkan*

Department of Chemical Engineering, The Ohio State University, Columbus, Ohio 43210

Received: January 13, 2002; In Final Form: April 21, 2002

The structural characteristics of supported MoO_x species inherent over a high TiO_2 content silica−titania mixed-oxide support (1:1 molar ratio), combined with the structural effects that are induced by an alkali promoter, are the primary focus of this investigation. The catalysts were prepared using a "one-pot" modified sol−gel/coprecipitation technique that distributes the molybdenum precursor throughout the Si/Ti support network as it forms during gelation. The Si/Ti 1:1 mixed-oxide support is in a state of nanodispersed titania (anatase) over silica. With the introduction of molybdenum and successive levels of alkali promoter, the dispersion of titania decreases as does the interaction of TiO_x species with silica. Concurrent with this change is the observation of an enhanced interaction of the MoO_x species with silica. Correlation is found among the propane ODH reactivity, the surface coverage of oxidic molybdenum species, and the nature of the Si/Ti support. ^{1}H-^{29}Si CP-MAS NMR data and DRIFT spectra taken in the hydroxyl stretching region (3000−3900 cm^{-1}) suggest that, with the addition of alkali, the three dimensionality of the silica support is changing to accommodate the change in MoO_x surface structure. The presence of potassium significantly alters the dispersion of titania and the electronic structure of the surface MoO_x domains, even before the formation of K-molybdate species is observed at higher K/Mo molar ratios. This electronic interaction is observed readily in the ESR spectrum of Mo(V) that is present in the dehydrated samples. Data suggest that surface-supported species, present as distorted octahedral MoO_x, become the most distorted at low alkali levels (K/Mo = 0.07). The MoO_x species at this level of alkali promotion, which experience a decrease in Lewis acidity, could tend to be more reactive toward electronegative $Si-O^-$ support ligands on the Si/Ti 1:1 support. The observed increase in propane ODH reactivity at low K/Mo molar ratios may be ascribed to a highly distorted structure sharing both titania and silica ligands.

Introduction

The partial oxidation and oxidative dehydrogenation (ODH) of light alkanes are topics of commercial and scientific interest because improved understanding of these reactions can lead to utilization of relatively inexpensive and abundant alkane resources. Consequently, since the 1980s, the conversion of light alkanes into more valuable organic compounds has been extensively studied.[1−5] The oxidation of light alkanes to alkenes occurs via parallel and sequential oxidation steps in which alkenes are primary ODH products whereas CO and CO_2 can form via either secondary combustion of alkenes or direct combustion of alkanes.[6−9]

Although it is generally accepted that the selective mechanism of propane ODH follows a Mars van Krevelen redox mechanism, there are many nonselective mechanistic steps that can possess several structural requirements, which can develop the observed reaction behavior in a quite complicated manner. Nonselective mechanisms can exist in which oxygen, from the lattice or activated from the gas phase, can be inserted into the hydrocarbon, and several reaction steps advance ultimately to form carbon oxides. For selective catalysts, there should exist an optimal balance in the oxygen activity, acid−base characteristics, and lattice diffusivity. It is therefore essential for a catalyst to possess a certain degree of structural complexity such as differing metal−oxygen bond strengths for an optimum combination of activity and selectivity. The oxides of V and Mo, through their multiple oxidation states and varying support interactions, offer such structural complexity to serve this purpose.[10] Over supported molybdenum and vanadium oxides, several isolated species may exist in the form of M═O, M−O−M, or M−O support bonds, where M is the transition metal of interest. The nature of the active oxygen species and redox properties will play a critical role in catalyst performance and will certainly depend on transition-metal loading, dispersion, and support effects.

One way to achieve the complex functionality and site isolation of a partial oxidation catalyst is to support the active metal oxide on a binary oxide support. Binary mixed oxides have been studied as catalyst supports in a variety of reactions including hydrotreating, selective oxidation, and the SCR of nitrogen oxides.[11−17] The mixed oxides including binary mixtures of alumina, zirconia, silica, or titania have received the most attention. In particular, the binary TiO_2/SiO_2 system, with its enhanced thermal/mechanical stability and high surface area, is considered to be an advanced material that could be an economically more attractive alternative for TiO_2.[18−20] Despite their application potential, the structural aspects of supported vanadium or molybdenum on these binary oxide supports are included in only a few studies. Ko et al. and Kumbhar[21,22] have shown that TiO_2/SiO_2 mixed oxides exert both direct and indirect support effects when used as supports for Ni catalysts. Further-

* To whom correspondence should be addressed. E-mail: ozkan.1@osu.edu. Tel: (614) 292-6623. Fax: (614) 292-3769.

10.1021/jp025512+ CCC: $22.00
Published on Web 06/06/2002

more, Baiker et al.[23] have proposed that by varying the TiO_2 content in the mixed oxides one can "tune" the interaction with VO_x species to form an optimal deNO_x catalyst. Catalysts composed of vanadium oxide species dispersed on TiO_2/SiO_2 (5−15% TiO_2)[24] and Al_2O_3/SiO_2 (0−10% Al_2O_3)[25] have recently been prepared and thoroughly characterized. It was concluded that the vanadium oxo species preferentially interact with the titania or alumina portions of the support. On the same samples, however, addition of VO_x to the support was found to consume some of the surface Si−OH hydroxyls, indicating that an interaction of VO_x with silica is not necessarily absent and several supported species may be present with different $Ti-O^-$ (or $Al-O^-$) and $Si-O^-$ ligands. Furthermore, it was the varying ratio of these ligands that was ascribed to significant changes in the reactivity of isolated vanadium oxide units. Because ODH reaction pathways on molybdenum- and vanadium-containing catalysts are similar,[26] it is plausible that, when supported on a binary oxide, the nature of dispersed MoO_x domains will exhibit characteristics similar to those of VO_x domains supported on a binary oxide.

The structural characteristics inherent over the high TiO_2 content silica−titania mixed-oxide support, combined with the structural effects that are induced by an alkali promoter, are the primary focus of this investigation. Alkali doping can also influence surface properties by preventing phase transformations, inhibiting sintering, inducing coordination changes, decreasing reducibility, and creating basic centers on the catalyst surface.[27−30] Our previous work has shown that the Mo/Si−Ti 1:1 catalysts are effective for the oxidative dehydrogenation (ODH) of propane. When promoted with alkali (K), the catalysts have shown a broad maximum in activity and selectivity according to the amount of alkali (K) promoter added. Although the catalysts exhibit this trend for propane ODH under a wide range of conditions, we were not able to reproduce the combination of high activities and selectivities reported earlier.[31] However, preparation of multiple batches of catalysts and testing under different experimental conditions have revealed that the activity trend with K/Mo ratio, that is, an initial increase in activity at low alkali content followed by a sharper decline, is unambiguous.

In this study, a series of potassium-promoted molybdenum catalysts (alkali/Mo molar ratio < 1) have been characterized by probing the surface molybdenum species and the physical−chemical properties of the Si/Ti support. The effect of the alkali level on the surface characteristics of the support has been examined. Surface areas were measured using the BET N_2 adsorption method. Characterization has been performed using laser Raman spectroscopy, X-ray photoelectron spectroscopy (XPS), transmission electron microscopy (TEM), and diffuse reflectance infrared Fourier transform spectroscopy (DRIFTS) to elucidate the surface/bulk structure and the nature of Si/Ti surface hydroxyl species. electron-spin resonance (ESR) was performed to probe the existence and nature of reduced or distorted MoO_x structures. ^{29}Si CP-MAS NMR was performed to observe the change in the silica network cross-linkage with the level of alkali doping.

Experimental Section

Catalyst Preparation. The catalysts were prepared using a modified sol−gel/coprecipitation technique. Ammonium heptamolybdate (AHM) (Mallinckrodt) and KOH (Fisher) were used for molybdenum and potassium precursors, respectively. For silica−titania mixed oxides and single oxides, tetraethyl orthosilicate (TEOS) (Aldrich) and titanium(IV) isopropoxide (TIPO) (Aldrich) were used. This sol−gel method is described as a "one-pot" sol−gel/coprecipitation that distributes the molybdenum precursor throughout the Si/Ti support network as it forms during gelation and is described in detail elswhere.[31] Synthesized catalysts are listed in Table 1. The samples were also compared to commercial silica (Cab-O-Sil). Samples 1−4 are supports prepared in the same manner as that for the catalysts, with the exception of commercial Cab-O-Sil silica. Catalysts 5−10 are a series of molybdate catalysts with an increasing K/Mo molar ratio at a constant (10 wt %) loading of Mo and a Si/Ti molar ratio of 1. BET surface area measurements and nitrogen adsorption−desorption isotherms were recorded using a Micrometrics AccuSorb 2100E instrument.

TABLE 1: Sol−Gel Catalysts and Support Materials

no.	composition	preparation	surface area (m^2/g)
1	SiO_2	sol−gel hydrolysis	620
2	SiO_2	Cab-O-Sil	380
3	TiO_2	sol−gel hydrolysis	31
4	Si/Ti 1:1	sol−gel hydrolysis	320
5	10% Mo/Si−Ti 1:1	coprecip., sol−gel	229
6	10% (K/Mo = 0.035)/Si−Ti 1:1	coprecip., sol−gel	164
7	10% (K/Mo = 0.07)/Si−Ti 1:1	coprecip., sol−gel	136
8	10% (K/Mo = 0.14)/Si−Ti 1:1	coprecip., sol−gel	121
9	10% (K/Mo = 0.3)/Si−Ti 1:1	coprecip., sol−gel	129
10	10% (K/Mo = 0.6)/Si−Ti 1:1	coprecip., sol−gel	65

Propane ODH Reaction Performance. Steady-state reaction experiments were carried out in a fixed-bed, quartz reactor that was operated at ambient pressure. A HP 5890 series II gas chromatograph equipped with FID and TCD detectors was used to perform separations and the analysis of reaction products online. Separations were performed using three columns: (1) Hayesep D (8 ft × $^1/_8$ in.) for hydrocarbons and partially oxygenated hydrocarbons, (2) Porapak Q (6 ft × $^1/_8$ in.), and (3) 5 Å molecular sieves (6 ft. × $^1/_8$ in.) for N_2, O_2, CO, CO_2, and H_2O. Catalyst samples ranging from 0.1 to 1.5 g were held in place by a quartz frit. The feed consisted of propane/oxygen/nitrogen at a flow rate of 25 cm^3/min. The concentration of the feed stream was maintained outside the flammability limits of propane/oxygen/nitrogen mixtures for all runs. The main products of the dehydrogenation reaction were propylene, carbon dioxide, carbon monoxide, and water. The product distributions maintained a carbon balance of 100% (± 5%). During catalytic reaction experiments, the dead volume of the quartz reactor was packed with quartz wool and ceramic beads to minimize any gas-phase effects that may occur in the presence of a catalyst.

Catalyst Characterization. X-ray diffraction patterns were obtained with a Scintag PAD-V diffractometer using Cu Kα radiation. TEM images and quantitative elemental analysis were performed on a Philips CM-300 FEG equipped with a light element EDS X-ray detector.

Raman spectra were recorded with a Dilor spectrometer using the 514.5-nm line of an Innova 300 Ar laser. Spectra were taken in the range 200−1800 cm^{-1} in the 180° backscattering mode with a Spectrum One CCD detector. Raman spectroscopy under dehydrated conditions was performed using a quartz in-situ flow cell that was capable of bringing the catalysts in contact with flowing gas at high temperatures. A portion of the prepared samples was recalcined at 550 °C for thirty minutes under pure O_2 and transferred into the Raman cell. Additional dehydration occurred at 350 °C for thirty minutes under a flow of dry 10% O_2/He, after which the cell was sealed. Spectra were taken under a 10% O_2/He atmosphere at room temperature.

X-ray photoelectron spectroscopy (XPS) of catalysts was performed with an ESCALAB MKII ESCA/Auger spectrometer

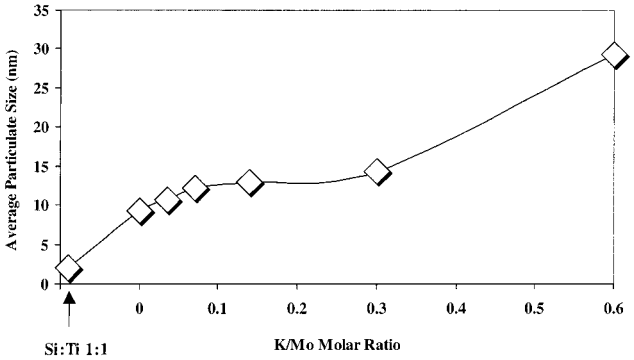

Figure 1. TiO_2 (anatase) particulate size as determined from X-ray diffraction line broadening.

operated at 14kV, 20mA using Mg Kα radiation. Spectra were corrected using the C 1s signal located at 284.6 eV.

The ^1H-^{29}Si CP-MAS NMR spectra were obtained on a Bruker 400DMX wide bore FT/NMR. A portion of the prepared samples was recalcined at 550 °C for thirty minutes under pure O_2 and maintained in the dehydrated state at 110 °C for 2 days prior to analysis. The data were acquired using a MAS of 5 kHz in a ZrO_2 rotor. The chemical shifts are reported relative to tetramethylsilane (TMS).

Diffuse reflectance infrared Fourier transform spectroscopy (DRIFTS) of the catalysts was performed using a Bruker IFS66 instrument equipped with a DTGS detector and a KBr beam splitter. Catalyst samples (2 wt % in KBr) were placed in a sample cup inside a Spectratech diffuse reflectance cell equipped with KBr windows and a thermocouple mount that allowed direct measurement of the surface temperature. Heating was performed under a flowing, dry helium atmosphere. KBr was used as reference. Spectra were averaged over 1000 scans in the mid-IR range ($400-4000cm^{-1}$) to a nominal 2 cm^{-1} resolution. Spectra were converted to Kubelka−Munk units. Deconvolution and area calculations of hydroxyl bands were performed using the GRAMS 32 software package.

Electron spin resonance (ESR) spectra were acquired on a Bruker ESP300 electron spin resonance spectrometer. For ESR spectrum taken under dehydrated conditions, a portion of the prepared samples was recalcined at 550 °C for 30 min under pure O_2 and maintained in the dehydrated state at 110 °C for 2 days prior to analysis. The spectra were obtained at room temperature with a Klystron frequency of 9.76 GHz at 2 mW power and 100 kHz magnetic field modulation.

Results and Discussion

Bulk Characterization. X-ray diffraction patterns were obtained on all catalyst samples. X-ray diffraction of the Si/Ti 1:1 support yielded a pattern characteristic of a silica−titania mixed oxide containing extra-framework anatase.[32] One broad peak with its center located at a *d* spacing of 3.59 Å was observed, which is the most intense diffraction line from anatase. This peak is indicative of a dispersed, nanosized anatase structure supported over amorphous silica. When the size of individual crystals is below 50 nm, a reasonably good measure of particle size can be determined from the broadening of diffraction lines measured at half of their maximum intensity.[33] Results of this measurement are shown in Figure 1. With the addition of molybdenum, the anatase diffraction peak becomes narrower, indicating a change in the dispersion and segregation of titania in the Si/Ti matrix. With the addition of potassium, the peak continues to narrow, indicating a higher degree of TiO_2 (anatase) segregation with the K/Mo molar ratio. With the

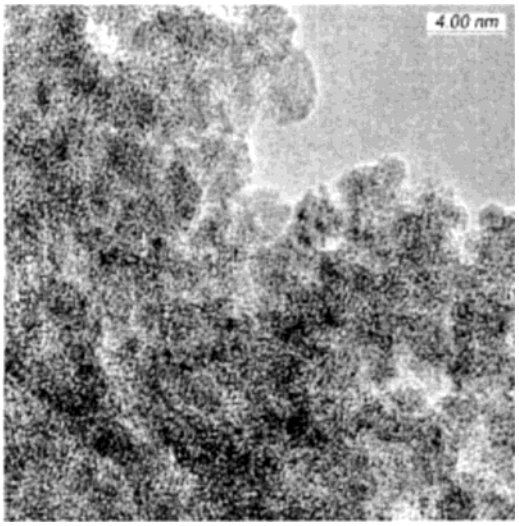

Figure 2. TEM micrograph of Si/Ti 1:1.

introduction of molybdenum to the Si/Ti 1:1 support, the particulate size increases from approximately 2 to 9 nm. The particulate size then slowly increases with the addition of K until a sharper increase is observed at K/Mo = 0.6. This value agrees with previous XPS data that has shown a continuous shift of the Ti $2p_{3/2}$ binding energy from that of TiO_x closely interacting with silica toward that of pure anatase.[31] This bulk structural change may be due to the higher pH of the "one-pot" synthesis medium with increasing potassium doping. The increasing basic conditions during preparation can have the effect of increasing condensation rates leading to larger particle size.[34] The pH of the preparation medium not only affects the support structure but also has a strong effect on the types of molybdenum species that are formed on the surface. However, the XRD patterns indicate that the molybdenum species are finely dispersed because no MoO_3 diffraction patterns were observed for any of the samples studies.

To observe the bulk structural changes associated with potassium addition, several TEM images of the samples were obtained. EDX analysis of the Si/Ti 1:1 support indicated a homogeneous dispersion of Si and Ti that closely matched the bulk atomic concentrations ("as-prepared" 46.25% Si and Ti). One of the TEM images obtained for Si/Ti 1:1 is shown in Figure 2. On all images obtained, an average particle size of 2 nm was observed with evidence of crystalline TiO_2 homogeneously distributed throughout the sample. However, with the addition of molybdenum to the Si/Ti 1:1 support, the larger size of the TiO_x domains in the sample was more readily observed, as indicated by the lattice fringes from crystalline TiO_2. These lattice fringes, with an average spacing of ∼3.3 Å, were more prominent than in the Si/Ti 1:1 support. On average, the overall particle size of the sample was observed to increase to 4.5−6 nm. EDX analysis over different regions revealed atomic concentrations fairly close to the "as-prepared" bulk values with only a few observances of TiO_2-rich regions. One such observation is shown in Figure 3 a (Si 38%, Ti 54%, Mo 8%) and b (Si 45%, Ti 46%, Mo 9%). EDX analysis over several regions also revealed a homogeneous distribution of molybdenum. With the addition of potassium (K/Mo = 0.07), further increase in the size of TiO_x domains is apparent by the presence of anatase lattice fringes as well as by the formation of hexagonal TiO_2 chips observed in the TEM image for an average particle size of 5−6 nm. EDX analysis provided evidence that Mo-rich regions exist in this sample. In Figure 4, the atomic concentrations are fairly close to the bulk values, with minor

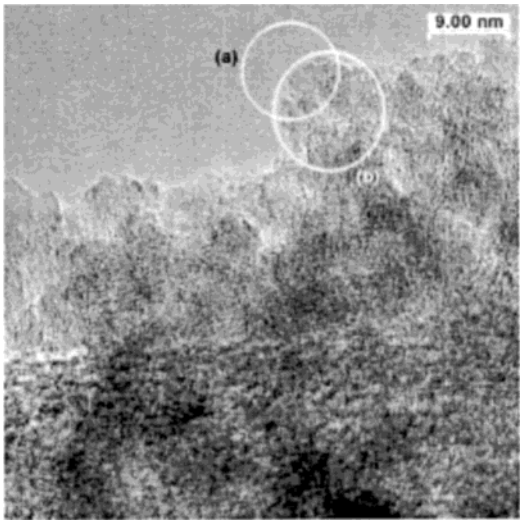

Figure 3. TEM micrograph of 10% Mo/Si−Ti 1:1. EDX analysis yielded region (a) Si 38%, Ti 54%, Mo 8%; region (b) Si 45%, Ti 46%, Mo 9%.

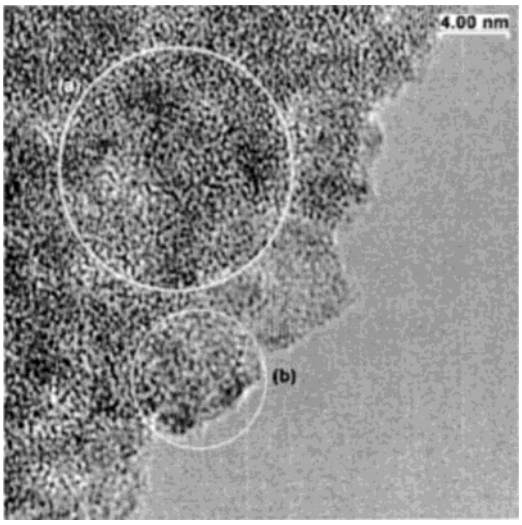

Figure 4. TEM micrograph of 10% (K/Mo = 0.07)/Si−Ti 1:1. EDX analysis yielded: region (a) Si 48%, Ti 40%, Mo 12%; region (b) Si 46%, Ti 47%, Mo 7%.

Mo-enriched regions observed (Figure 4a (Si 48%, Ti 40%, Mo 12%) and b (Si 46%, Ti 47%, Mo 7%)). However, there were several small, dark-contrast regions indicative of Mo segregation. Figure 5 a depicts such a region with atomic concentrations of Si 26%, Ti 27%, and Mo 47%. Figures 2−5 are representative of the complete analysis of the K/Mo = 0.07 particles, in which all Mo-rich regions analyzed showed an equal distribution of Si and Ti. Figure 5b illustrates that much of the sample maintained a distribution of components close to the as-prepared values: Si 44%, Ti 50%, Mo 6%. In Figure 5c, the analysis was performed at an interface between an SiO_2-rich region and a TiO_2-rich region. The white rift apparent in the Figure is a result of damage to the sample caused by several repeated EDX analyses, and the image was taken post-EDX analysis. Atomic concentrations at this SiO_2/TiO_2 interface did not show segregation of molybdenum (Si 45%, Ti 47%, Mo 8%).

When the level of alkali doping is increased to K/Mo = 0.3, a dramatic change was observed in particle size. Particles of differing geometries and sizes were observed, with the size range of the largest particles equal to about 40 nm. Figure 6 shows one set of the several SiO_2 and TiO_2 agglomerates observed, where the TiO_2-rich agglomerate is the oval-shaped particle on

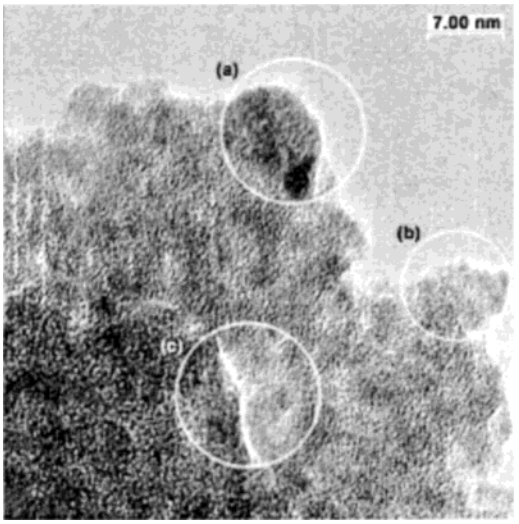

Figure 5. TEM micrograph of 10% (K/Mo = 0.07)/Si−Ti 1:1. EDX analysis yielded region (a) Si 26%, Ti 27%, Mo 47%; region (b) Si 44%, Ti 50%, Mo 6%; region (c) Si 45%, Ti 47%, Mo 8%. White rift in region (c) caused by extended EDX analysis.

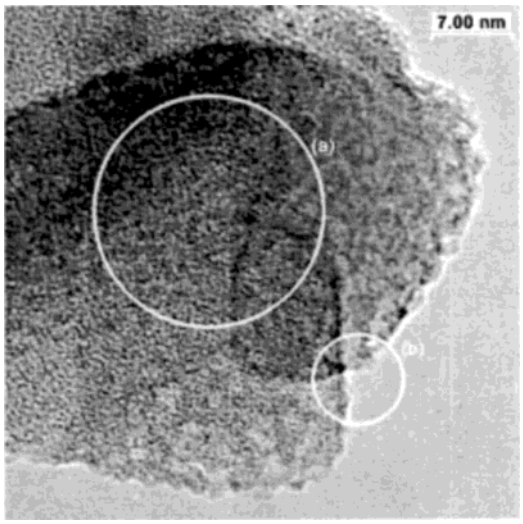

Figure 6. TEM micrograph of 10% (K/Mo = 0.3)/Si−Ti 1:1. EDX analysis yielded region (a) Si 59%, Ti 37%, Mo 4%; region (b) Si 44%, Ti 51%, Mo 5%.

the right in the Figure. However, analysis over SiO_2-rich regions, TiO_2-rich regions, and SiO_2/TiO_2 interface regions did not show an increase in molybdenum concentration in Figure 6 or during the entire analysis (Figure 6a (Si 59%, Ti 37%, Mo 4%) and b (Si 44%, Ti 51%, Mo 5%)). It is apparent from Figure 7 that the bulk nature of the catalyst at alkali level K/Mo = 0.3 is much different than that of the K/Mo = 0 catalyst because of the very large degree of TiO_2 segregation observed.

Results from TEM analysis agree with the XRD patterns showing how TiO_x domains that are initially evenly dispersed over silica increase in size and crystallinity with the K/Mo molar ratio. At the alkali level of K/Mo = 0.3, a very large segregation of titania is observed. However, even though EDX analysis indicated that a high agglomeration of Ti exists, there was a substantial amount of silica present in TiO_2 regions. Furthermore, a substantial amount of titania was also found to exist in silica-rich regions. Within experimental error, the bulk characterization provided by EDX analysis did not provide evidence that molybdenum is preferentially located over silica-rich, titania-rich, or Si/Ti interfacial regions of the support on any of the samples studied. Thus, the analysis suggests that any

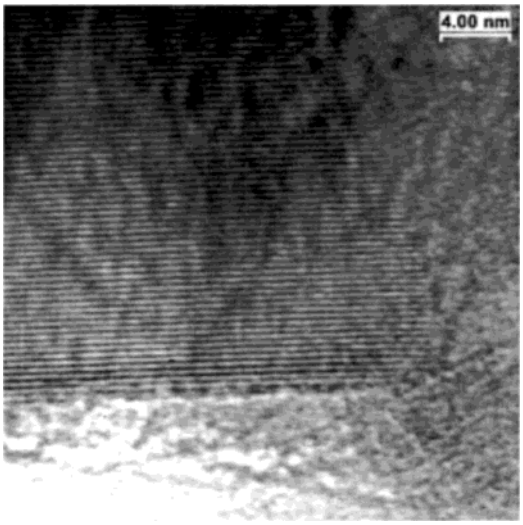

Figure 7. TEM micrograph of ~40-nm TiO_2 particle in 10% (K/Mo = 0.03)/Si−Ti 1:1.

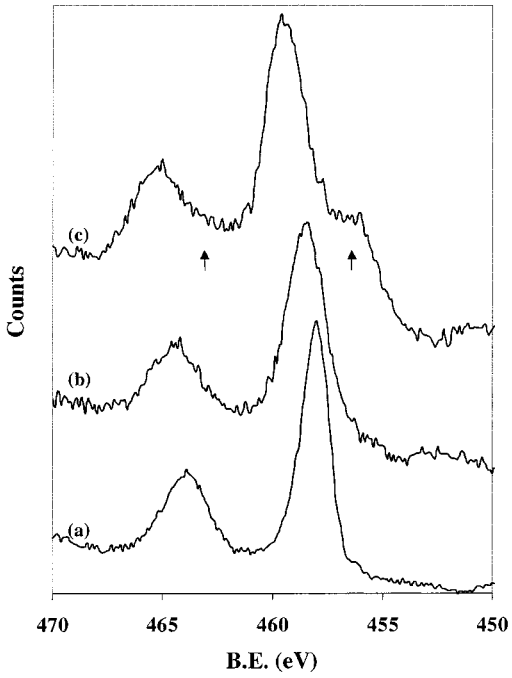

Figure 8. Ti 2p XPS spectra for Ti-containing support materials. (a) TiO_2 (sol−gel), (b) SiO_2−TiO_2 1:1 molar (physical mixture), (c) Si/Ti 1:1 support.

preferential interaction of Mo with TiO_2 or SiO_2 that may exist would have to be a surface effect.

X-ray Photoelectron Spectroscopy (XPS). To characterize the surface of the Si/Ti 1:1 support, a series of XPS experiments was performed to compare the support to SiO_2 (sol−gel), TiO_2 (sol−gel), and their physical mixtures. The Ti 2p XPS spectra for the support materials are shown in Figure 8. The Ti $2p_{3/2}$ binding energy of the sol−gel-prepared TiO_2 is 458.0 eV (Figure 8a). The spectrum obtained from the physical mixture is very similar to that of pure TiO_2, although it appears that a slight interaction may exist between mixtures of SiO_2 and TiO_2 because this binding energy is seen to shift to a slightly higher value (458.4) in the physical mixture (Figure 8b). In Figure 8c, it can be seen that the Ti $2p_{3/2}$ binding energy shifts much more pronouncedly, to 459.2 eV, for the Si/Ti 1:1 support. The large difference between the binding energy of TiO_2 (sol−gel) and

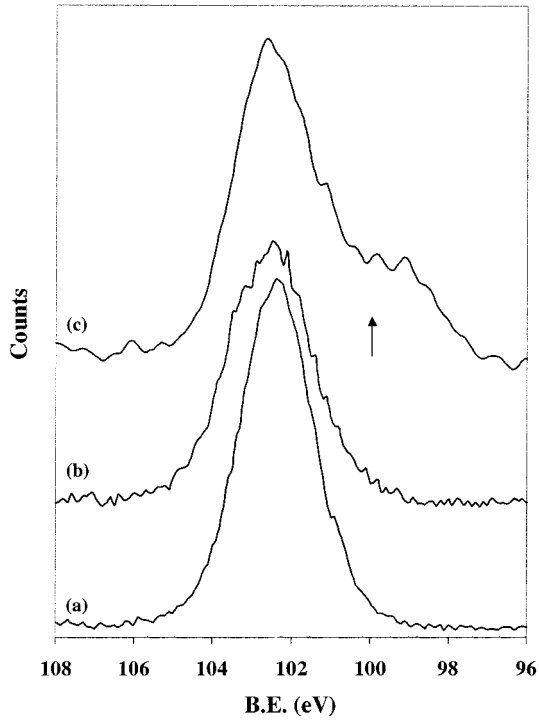

Figure 9. Si 2p XPS spectra for Si-containing support materials. (a) TiO_2 (sol−gel), (b) SiO_2−TiO_2 1:1 molar (physical mixture), (c) Si/Ti 1:1 support.

that of the Si/Ti support is indicative of TiO_x closely interacting with the silica surface.[35]

There is also a pronounced feature in the Ti 2p spectrum of the Si/Ti support located at 456.5 eV. This feature may be associated with Ti atoms present in Ti−O−Si. Fernandez et al.[36] have assigned an XPS feature at 456.4 eV to a reduced titania site (Ti^{3+}). Whereas this site remains as a possibility, it is more likely that the Ti site responsible for the XPS feature in Figure 8c may be an electron-rich species produced by integration of Ti into the silica network at boundaries, not at a fully reduced site. In TiO_2-rich samples of Si/Ti, the Ti^{4+} in Ti−O−Si shares more negative charges from the oxygen in SiO_2 than from the oxygen in the bulk.[37] Furthermore, it has been stated that, in phase-separated SiO_2/TiO_2 samples such as those under investigation here, Si−O−Ti bonds are likely to form at interface boundaries between SiO_2 and TiO_2.[38]

The Si 2p XPS spectra (Figure 9) shows a peak located at ~102.3 eV, which is characteristic of SiO_2 that does not shift positions between the support samples studied. There is an additional feature in the Si 2p spectrum of the Si/Ti 1:1 support (Figure 9c) that is present as a shoulder around ~99.0 eV. This feature is assigned to the Si atoms of Ti−O Si. Further evidence for Si−O−Ti bonds is obtained by examining the O 1s XPS spectra of the support samples presented in Figure 10. O 1s from SiO_x is located at ~533.4 eV, whereas the signal from TiO_x is located around 530 eV. Si−O−Ti species can exhibit an O 1s band between those of SiO_2 and TiO_2 around 532 eV, making the peak significantly broadened. The O 1s spectra of the Si/Ti 1:1 support is very similar to that reported in the literature by Stakheev et al.,[39] who have observed an identical spectrum over a 50% TiO_2/SiO_2 sample.

Raman Spectroscopy. Raman spectra have been obtained over the Si/Ti 1:1 support and have been compared to different preparations of pure silica in Figure 11. It was found that the dehydrated Si/Ti 1:1 surface possess Raman bands at 605, 800, 916, and 1080 cm^{-1}. The bands at 605 and 800 cm^{-1} are

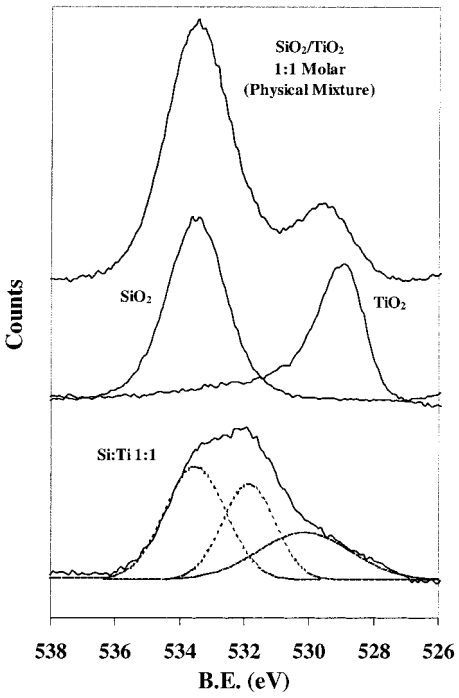

Figure 10. O 1s XPS spectra for support materials. TiO_2 (sol−gel), SiO_2−TiO_2 1:1 molar (physical mixture), Si/Ti 1:1 support.

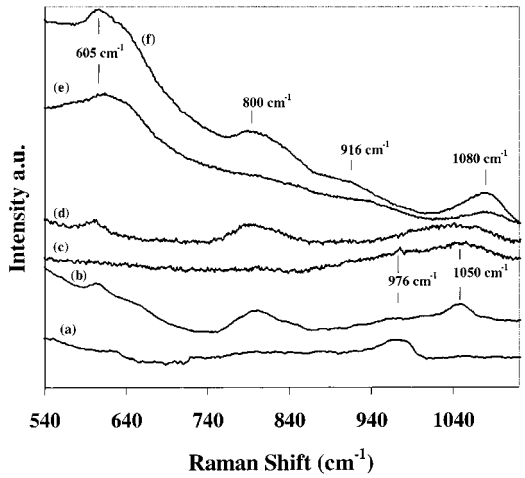

Figure 11. Raman spectra of SiO_2 and Si/Ti 1:1 support. Ambient conditions: (a) SiO_2 (Cab-O-Sil), (c) SiO_2 (sol−gel), (e) Si/Ti 1:1. Dehydrated conditions: (b) SiO_2 (Cab-O-Sil), (d) SiO_2 (sol−gel), (f) Si/Ti 1:1. Spectra of dehydrated samples taken under a 10% O_2/He atmosphere at room temperature.

attributed to the silica surface whereas the bands located at 916 and 1080 cm^{-1} have been assigned to perturbed silica vibrations that are indicative of Ti−O−Si bonds.[20,40−42] We conclude that the Si/Ti 1:1 support is in the state of nanocrystalline TiO_x dispersed over silica.

To differentiate between the Raman bands arising from the Si/Ti support and those from surface-supported molybdate species, Raman spectra were recorded under ambient and dehydrated conditions over silica (sol−gel), which was prepared in the same way that the catalysts were, fumed silica (Cab-O-Sil), and the Si/Ti 1:1 support and were compared in Figure 11. On a pure silica sample, a distinct band that corresponds to surface silanols has been reported to occur between 971 and 976 cm^{-1}.[43,44] Although not expected to interfere at the somewhat high Mo loading of 10 wt %, this band can be convoluted with the Mo═O band of the MoO_x species that is

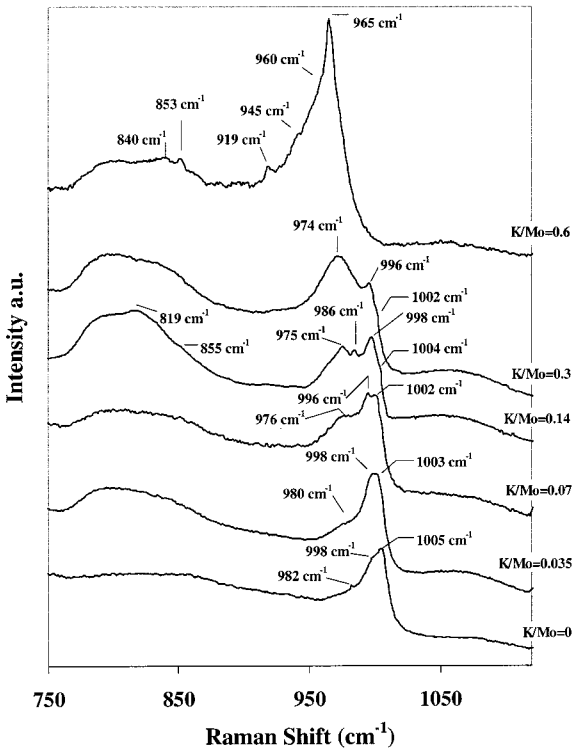

Figure 12. Raman spectra of 10% Mo/Si−Ti 1:1 catalysts with differing K/Mo molar ratios. Spectra taken under 10% O_2/He atmosphere at room temperature under dehydrated conditions.

supported on silica at low Mo loadings. On 6.4% Mo/SiO_2, Williams et al.[45] have observed this Raman band on dehydrated samples at room temperature. After heating to 550 °C under oxygen, the Mo═O stretching frequency was observed at 994 cm^{-1} together with the broader silanol band at 971 cm^{-1}. After cooling to room temperature under oxygen, the Mo═O and silanol peaks shifted to 998 and 977 cm^{-1}, respectively. The authors stated that, over 0.1−10 wt % loading of Mo over silica prepared by a variety of precursors, the terminal Raman band was shifted to 994−998 cm^{-1} upon dehydration. This shift occurred for those samples that did not display the Mo−O−Mo bridging mode associated with crystalline MoO_3.

As seen in Figure 11, bands associated with surface silanols are not observed in the Si/Ti 1:1 support under ambient or dehydrated conditions. However, in the spectrum of SiO_2 (sol−gel) under ambient conditions, the band is present as a small, sharp feature at 976 cm^{-1} that disappears upon dehydration. In contrast, the Cab-O-Sil sample exhibits a much broader silanol band at the same location, which also disappears upon dehydration. We therefore conclude that there should be no Raman bands arising from the silanols that would cause a misinterpretation with Mo═O vibrations present on the dehydrated Si/Ti 1:1 support. The importance of this conclusion will be discussed in the subsequent text.

Raman spectra of the alkali-promoted Mo/Si−Ti 1:1 catalysts, taken under dehydrated conditions, are shown in Figure 12 in the molybdenum−oxygen (Mo═O and Mo−O−Mo) vibration region. Broad bands associated with crystalline TiO_2 limit the detection of MoO_x species below 640 cm^{-1}. Present in all the samples is a broad feature at 800 cm^{-1} that it attributed to the silica of the support. There are several discernible vibrations observed for each sample in the range 950−1005 cm^{-1}. Additionally, there are features present in the 780−850 cm^{-1} region for K/Mo = 0.14 and 0.6 catalysts. In general, bands in the range 750−950 cm^{-1} are attributed to the antisymmetric

stretching of Mo−O−Mo bonds or the symmetric stretch of $(-O-Mo-O-)_n$ bonds, whereas bands in the range 950−1050 cm^{-1} can be attributed to the stretching mode of Mo═O bonds.[46] There was no evidence of crystalline MoO_3 on any of the samples. However, as the alkali level reaches K/Mo = 0.6, there is evidence of the crystallinity of alkali molybdate species, possibly K_2MoO_4 and $K_2Mo_2O_7$, indicated by several bands between 840 and 960 cm^{-1}.[47,48] In fact, previous XPS data has indicated that much of the MoO_x of this catalyst is present in a tetrahedral, K-molybdate matrix.[31] Contributions to the Mo═O stretching frequency of 10% Mo/Si−Ti 1:1 appear at 982, 998, and 1005 cm^{-1}. With increasing K/Mo molar ratio, the band at ∼1005 cm^{-1} is seen to diminish in intensity relative to that of the lower-frequency bands and appears only as a shoulder in the K/Mo = 0.14 and 0.3 catalysts. In parallel with the decrease of the ∼1005 cm^{-1} band with K/Mo ratio is the increase of the band located at 996−998 cm^{-1} up to K/Mo = 0.3. In addition, a broad feature observable in K/Mo = 0 around 980 cm^{-1} is seen to grow in intensity with K/Mo molar ratio until a broad peak at 974 cm^{-1} is observed at K/Mo = 0.3. Overall, the multiple bands associated with isolated terminal Mo═O stretching vibrations are observed to shift with K/Mo ratio to lower wavenumbers. Shifts in the Mo═O Raman frequency are related to changes in bond length[49] and could result from an enhanced interaction with the support or from the introduction of K-containing species. Similar Mo═O band shifts were ascribed, on dehydrated Cs-promoted Mo/ZrO_2 catalysts, to the altering of electronic properties of MoO_x domains with the addition of small amounts of alkali that did not form detectable quantities of alkali molybdates.[50] However, for similar Raman spectra observed for a set of dehydrated, sodium-doped Mo/SiO_2 catalysts,[51] it was stated that the observed increase in intensity in the wavenumber region ∼940−990 cm^{-1} was due to the formation new molybdate species. Thus, it can be envisioned that the observed changes in Mo═O vibrations can arise from both an electronic interaction with potassium at small alkali content and the formation of alkali molybdates at higher K/Mo ratios.

There is a scarcity of data in the literature on Raman bands arising from surface-supported molybdenum species under dehydrated conditions, especially for those arising from molybdate species supported on the binary oxides of silica−titania. However, Wachs[49] has summarized the Raman spectroscopy results, under dehydrated conditions, of Mo/SiO_2 and Mo/TiO_2 prepared by several preparation methods and has stated that Mo═O Raman bands of surface-supported MoO_x on titania appear in the range 998−1001 cm^{-1}. On silica under dehydrated conditions, these bands are reported to be a function of weight loading and appear in the range 975−990 cm^{-1}. However, in another study[44], bands arising from dehydrated surface-supported MoO_x species on silica were observed up to 998 cm^{-1}. The data in the literature suggest that it may be possible to interpret the Raman spectrum of MoO_x supported over binary oxides to gain qualitative information as to whether MoO_x preferentially interacts with one of the oxide domains by incorporating different support-O bonds. Therefore, in parallel with the observed changes in Raman spectra being assigned to an electronic interaction with potassium, the Raman spectra of Figure 12 can also be interpreted in terms of the MoO_x interaction with the support. In these terms, an increasing interaction with silica (increase in the bands 970−998 cm^{-1} with a decrease in the band ∼1005 cm^{-1}) can be envisioned with the addition of potassium. These bands appear to be present in equal proportion on the K/Mo = 0.035 and 0.07 catalysts.

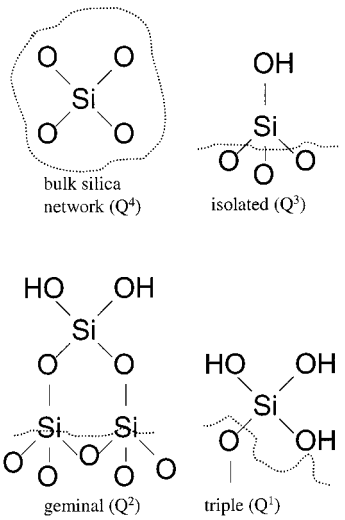

Figure 13. Silica species responsible for contributions to observed ^1H-^{29}Si CP-MAS NMR signals.

Further support for the proposal that MoO_x could be increasingly interactive with silica comes from the fact that the bands located at 998 and 977 cm^{-1} at higher K/Mo molar ratios are virtually identical to those reported for dehydrated β-silicomolybdic acid supported on silica.[52−53]

It appears that with the electronic effect of potassium the MoO_x species experience a greater interaction with silica whereas that with titania decreases. Raman bands that could be associated with both types of species become overshadowed by the formation of new molybdate species at higher K/Mo ratios (≥0.3). However, the exact structure cannot be assigned solely on the basis of Raman Mo═O positions because several phenomena must be considered simultaneously. XRD and TEM results have shown the dynamic nature of TiO_x dispersion with the K/Mo molar ratio. Together with the interaction of potassium with the supported molybdate species, the question arises as to how the combined phenomenon of the support structure and alkali interaction affects the dispersion of MoO_x over the binary oxide. Furthermore, its has been pointed out that when supported on binary oxides, transition-metal oxides are capable of sharing more than one type of support-O bond.[24−25] At this point, the effect of potassium on the number and kind of support-O−Mo ligands remains unclear. However, withstanding these complications, Raman spectroscopy does indicate that supported $K-MoO_x$ species exist in several types of structural configurations simultaneously and rather uniformly over Si/Ti 1:1.

^1H-^{29}Si CP-MAS NMR. CP-MAS ^{29}Si NMR spectroscopy can be used to characterize the structure of silica networks and has been used to characterize SiO_2/TiO_2 mixed oxides.[54−56] In single-pulse ^{29}Si NMR, both −OTi and −OH groups are reported to affect the silicon nucleus in a similar manner. However ,using ^1H-^{29}Si cross-polarization, the most likely candidates for signal enhancement are the SiOH groups.[56] These sites are depicted in Figure 13 with the corresponding Q^n notation, where *n* represents the number of Si−O ligands around each Si nucleus. The presence of adsorbed water may affect the signal enhancement by increasing the relaxation time of the protons involved in cross-polarization;[57] therefore, samples were recalcined at 550 °C for 30 min and maintained in the dehydrated state before analysis. Figure 14 shows the ^1H-^{29}Si CP-MAS NMR spectrum of the K/Mo catalysts. Contributions from the silicon nuclei show Gaussian peaks at approximately −109 ppm (Q^4), −101 ppm (Q^3), −92 ppm (Q^2), −84 ppm (Q^1). The relative contributions of these structural sites were

TABLE 2: Chemical Shifts of (K/Mo)/Si−Ti 1:1 Catalysts

	Q4		Q3		Q2		Q1	
sample	ppm	%	ppm	%	ppm	%	ppm	%
10% Mo/Si−Ti 1:1	−110	58.0	−101	36.6	−92	5.4		
10% (K/Mo = 0.0035)/Si−Ti 1:1	−110	61.2	−101	30.2	−93	8.3	−83	0.3
10% (K/Mo = 0.07)/Si−Ti 1:1	−110	66.9	−101	24.8	−93	8.3		
10% (K/Mo = 0.143)/Si−Ti 1:1	−110	60.4	−101	30.9	−93	8.7		
10% (K/Mo = 0.3)/Si−Ti 1:1	−110	55.8	−101	36.3	−92	7.1	−85	0.7
10% (K/Mo = 0.6)/Si−Ti 1:1	−110	51.0	−101	40.0	−92	8.7	−85	0.3

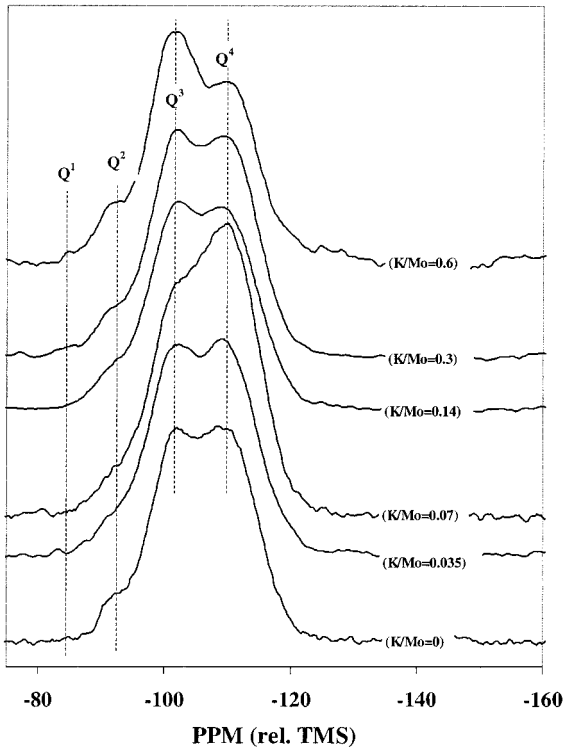

Figure 14. ^{1}H-^{29}Si CP-MAS NMR spectra of 10% Mo/Si−Ti 1:1 catalysts with differing K/Mo molar ratios.

calculated from deconvoluted, integrated areas and are presented in Table 2. As the data show, Q^4 sites are the dominant species present in all samples, indicating a well-developed silica network. However, 30−40% of the silicon nuclei are seen to contribute to the Q^3 sites of the silica network.

The ratios among different Q^n sites are often used to ascertain the degree of silica polymerization.[57] To examine the change in the silica network, the percentage contribution of Q^3 sites (free hydroxyls) and the ratio $Q^2/(Q^2+Q^3)$ are plotted in Figure 15 as a function of K/Mo molar ratio. As Figure 15 indicates, there is a pronounced minimum in the signal corresponding to free hydroxyl groups (Q^3) that occurs for the K/Mo = 0.07 sample. Furthermore, the ratio of geminal hydroxyl groups (Q^2) to the total hydroxyl content is found to reach a maximum over the same sample. The NMR data show that with the K/Mo molar ratio the nature of the silica surface changes. Previous data have shown that TiO_x species continuously segregate from the surface with increasing K/Mo ratio and reach a relatively large particle size at K/Mo = 0.3. Thus, it is expected that the interaction of TiO_x domains with the hydroxyls of silica decreases continuously with K/Mo ratio. It is therefore most likely that, as K/Mo increases, the change in the silica surface arises from the increasing interaction of MoO_x with the surface hydroxyl groups. The type of molybdate species responsible for such an interaction and whether this species shares different support-O ligands remain unclear. However, the data agree with the Raman results

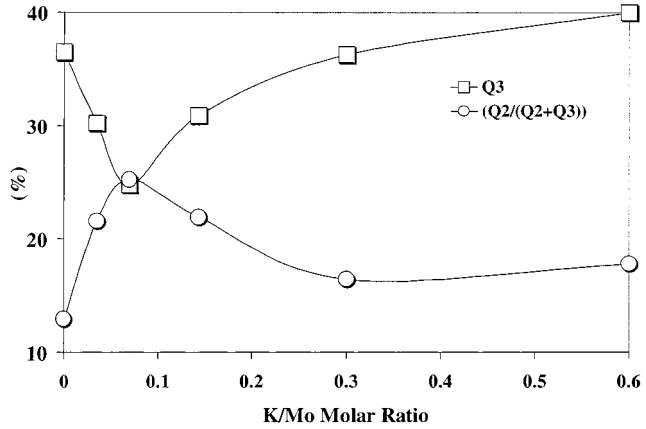

Figure 15. Variation in Q3 percentage (free hydroxyls) and Q2/(Q3 + Q2) percentage (of geminal hydroxyls) with K/Mo molar ratio.

presented previously that have suggested increased interaction of molybdenum with silica before the onset of alkali−molybdate formation.

Diffuse Reflectance Infrared Fourier Transform Spectroscopy (DRIFTS). High-resolution IR spectra can be used to ascertain the presence and relative quantity of the same isolated and geminal hydroxyl groups that were detected in the ^{1}H-^{29}Si CP-MAS NMR spectra.[58] To corroborate the information obtained from NMR spectroscopy, a series of DRIFTS experiments were performed over the K/Mo catalysts. The IR bands from surface hydroxyls were recorded for all samples in the range 3000−3900 cm^{-1} at temperatures of 25, 50, 100, 150, and 200 °C. For the sake of conciseness, only the results for K/Mo = 0, 0.07, and 0.3 are shown in Figure 16. For each sample, the IR bands associated with free hydroxyl groups are located from 3745−3747 cm^{-1}, whereas those from geminal hydroxyl groups are resolved from 3739−3740 cm^{-1}.[58,59] Broad and convoluted bands at wavenumbers ≤3730 cm^{-1} arise from weakly adsorbed water and are observed in the room-temperature spectrum. Hydroxyl species arising from Ti−OH were not observed in any of the samples at any temperature and are reported to occur at a maximum wavenumber of 3716 cm^{-1}.[60] Upon examination of Figure 16, it can be seen that K/Mo = 0.07 possesses a relatively weaker contribution from free hydroxyls (Figure 16b) than do the other samples. As the temperature is raised to 200 °C from room temperature, differences are observed in the relative quantities of free and geminal hydroxyl groups present on the samples. To compare with the NMR data, the hydroxyl bands were deconvoluted, and relative ratios (free/geminal) of the hydroxyl content were calculated for the K/Mo catalysts. Results are plotted in Figure 17 along with the ratio obtained from the NMR data (Q^3/Q^2). As can be seen, DRIFTS results are in very good agreement with the ratios obtained from NMR, showing a minimum amount of free hydroxyl species present at the low alkali level of K/Mo = 0.07. The ratios calculated from DRIFTS data obtained at higher temperatures exhibit identical trends (not shown).

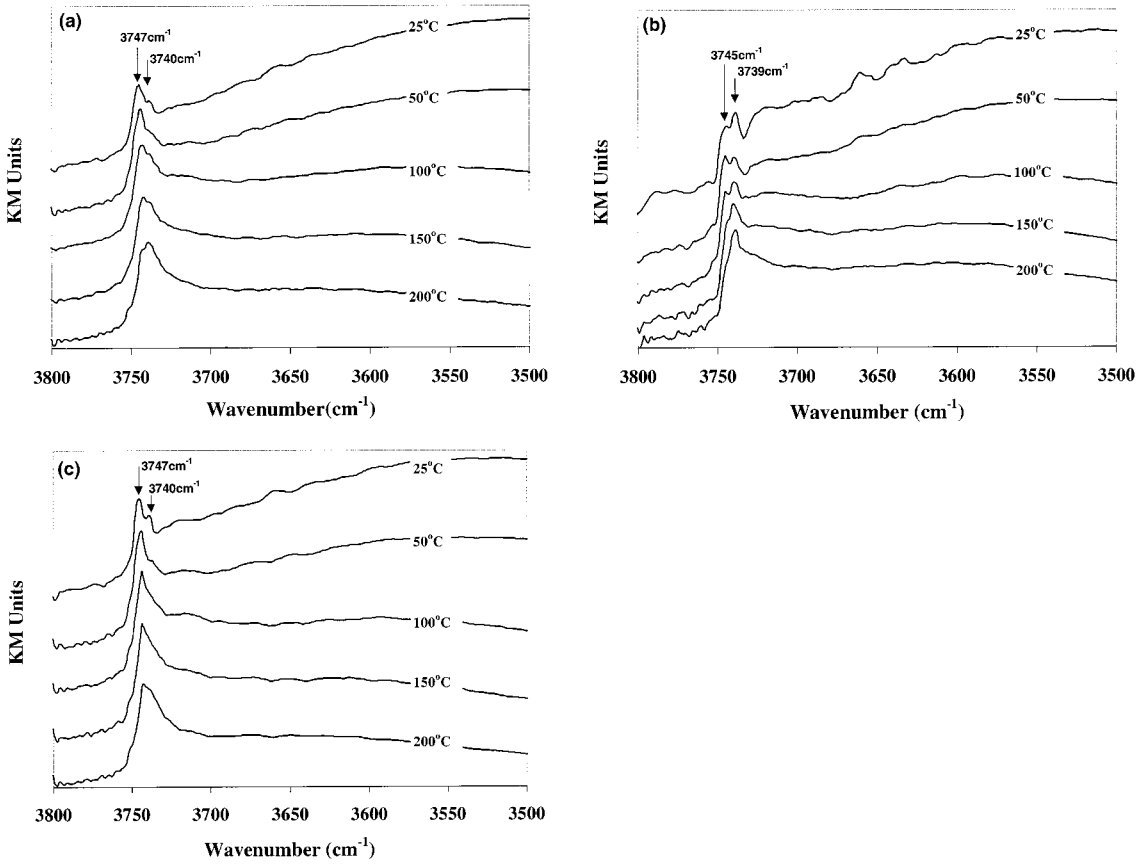

Figure 16. IR bands from surface hydroxyls for (a) K/Mo = 0, (b)K/Mo = 0.07, and (c) K/Mo = 0.3 catalysts at varying temperatures.

Electron Spin Resonance Spectroscopy (ESR). ESR techniques have been widely used to obtain insight into many aspects of the catalysis and surface chemistry of metal oxide surfaces.[61] In particular, calcination of MoO_x catalysts at high temperatures can lead to the formation of paramagnetic Mo(V) centers[62] that can be studied to probe the local environment of the surface-supported species. ESR spectra were recorded, at room temperature, on ambient-exposed and dehydrated K/Mo catalysts and the Si/Ti 1:1 support (Figures 18 and 19). A small signal from the superoxide ion (O_2^-) was the only signal detected on the Si/Ti 1:1 support (not shown) with a characteristic average g value of 2.011.[63] The structural assignment of this species cannot be directly determined because the superoxide ion can exist and be stabilized both in extra-framework TiO_2[63] (TiO_x not incorporated into silica) and in silica domains[61].

All ambient-exposed samples reveal asymmetric ESR signals associated with Mo(V) and, to a lesser extent, the superoxide ion O_2^- (Figure 18). The associated g tensor for Mo(V) is seen to change slightly among the ambient-exposed K/Mo catalysts (Table 3), whereas that of O_2^- remains fairly constant at g = 2.011. The spectra of Figure 18 are characteristic of Mo(V) in a state of *nonaxial* symmetry. The adsorption of atmospheric water can have a significant effect on the dispersion and coordination of MoO_x domains and thus the ESR spectrum. Therefore, the same experiment was performed over the K/Mo catalysts under dehydrated conditions (Figure 19). A noticeable broadening of the signal appears upon dehydration without substantial loss of intensity. The removal of adsorbed water can cause a decrease in the separation between Mo(V) ions and a consequent broadening of the ESR line widths.[64] The broad spectrum of Figure 19 is indicative of Mo(V) in a dehydrated oxide matrix.[64,65] After dehydration, the spectra in Figure 19 become more symmetric in nature (or quasi-axial[66]). However,

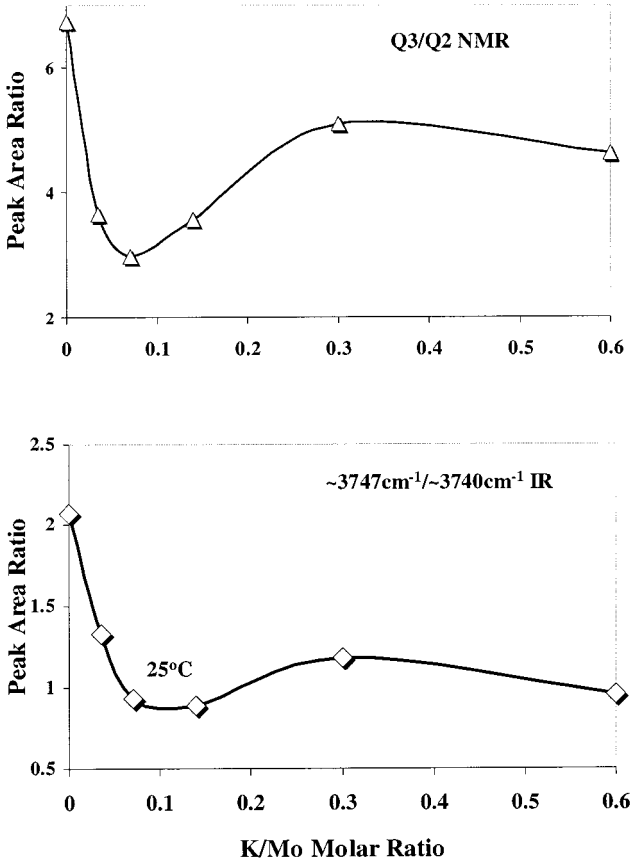

Figure 17. Comparison of NMR and DRIFTS ratios of free/geminal hydroxyls on 10% Mo/Si−Ti 1:1 catalysts with differing K/Mo molar ratios.

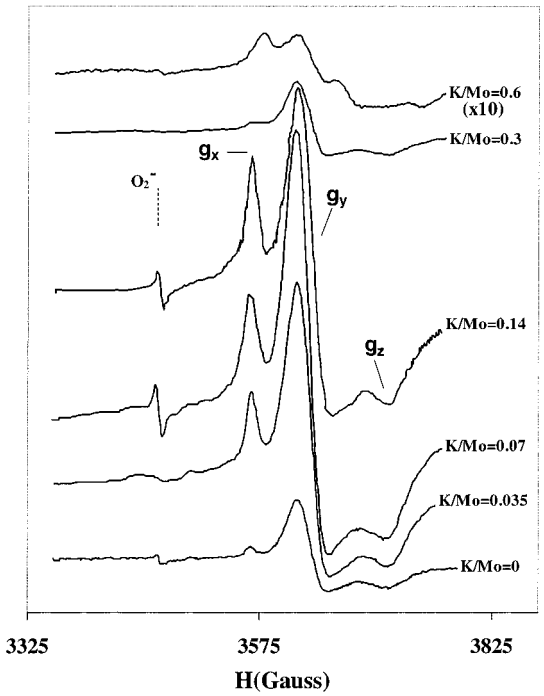

Figure 18. ESR spectra of 10% Mo/Si−Ti 1:1 catalysts with differing K/Mo molar ratios under ambient conditions.

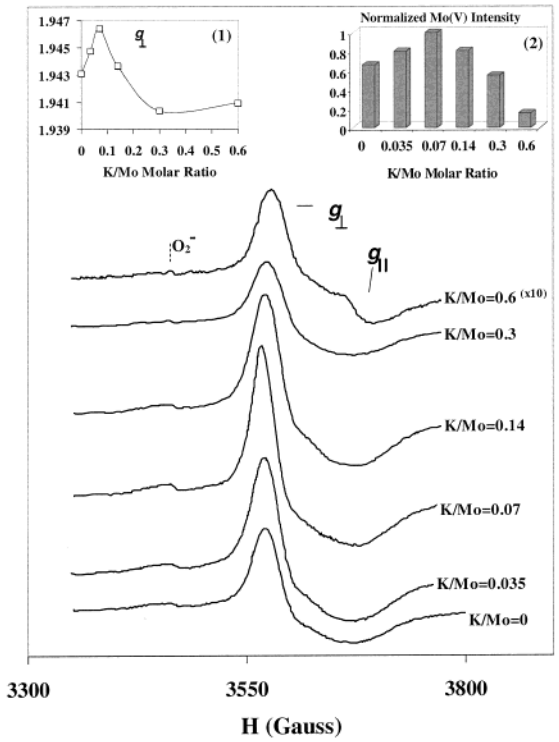

Figure 19. ESR spectra of 10% Mo/Si−Ti 1:1 catalysts with differing K/Mo molar ratios under dehydrated conditions. (1) Variation of g (perpendicular) with K/Mo molar ratio. (2) Variation of normalized signal intensity with K/Mo molar ratio.

the possibility remains that there could be a mixture of Mo(V) signals contributing to the observed spectra, which is especially true of the spectrum that corresponds to the K/Mo = 0.6 sample. Assuming quasi-axial spectra, parallel and perpendicular parameter values can be defined as $g_\perp = (g_x + g_y)/2$ and $g_{II} = g_z$. The $g_\perp$ and g_{II} values of Mo(V) in the dehydrated K/Mo samples are presented in Table 3. The $g_\perp$ values are seen to go through a maximum at K/Mo = 0.07, and this trend is depicted as inset 1 in Figure 19. The variation of integral intensity calculated from the spectra in Figure 19 is included as inset 2.

TABLE 3: *g* Tensor Mo(V) in (K/Mo)/Si−Ti 1:1 Catalysts

ambient conditions	catalyst	g_x	g_y	g_z
	10% Mo/Si−Ti 1:1	1.956	1.930	1.893
	10% (K/Mo = 0.035)/Si−Ti 1:1	1.955	1.929	1.891
	10% (K/Mo = 0.07)/Si−Ti 1:1	1.956	1.930	1.895
	10% (K/Mo = 0.14)/Si−Ti 1:1	1.956	1.929	1.890
	10% (K/Mo = 0.3)/Si−Ti 1:1	1.954	1.929	1.895
	10% (K/Mo = 0.6)/Si−Ti 1:1	1.949	1.928	1.867

dehydrated conditions	catalyst	$g_\perp$	g_{II}
	10% Mo/Si−Ti 1:1	1.943	1.900
	10% (K/Mo = 0.035)/Si−Ti 1:1	1.945	1.900
	10% (K/Mo = 0.07)/Si−Ti 1:1	1.946	1.895
	10% (K/Mo = 0.14)/Si−Ti 1:1	1.944	1.907
	10% (K/Mo = 0.3)/Si−Ti 1:1	1.940	1.905
	10% (K/Mo = 0.6)/Si−Ti 1:1	1.941	1.885

The g values for different coordination environments of Mo(V) are reported in the literature as follows: six-coordinate Mo(V), $g_\perp = 1.944$ and $g_{II} = 1.892$; five-coordinate Mo(V), $g_\perp = 1.957$ and $g_{II} = 1.866$; and four-coordinate Mo(V), $g_\perp = 1.926$ and $g_{II} = 1.755$.[61,67−69] Because the perpendicular component is expected to be the most sensitive to the coordination of the isolated MoO_x species, the data indicate that with the addition of potassium there is a change in the coordination sphere (six-coordinate distorted toward five-coordinate) of the Mo(V) species that reaches a maximum at K/Mo = 0.07. Furthermore, the integral signal intensity follows the same trend. The g values of the K/Mo = 0.3 and 0.6 samples indicate a distortion in the opposite direction toward that of a four-coordinate Mo(V) species that can arise from the formation of K−molybdates. Furthermore, the symmetry of the spectrum for the K/Mo = 0.6 sample is significantly altered compared to that of the sample with no K component. This behavior is a likely result of the formation of more tightly packed K_2MoO_4 and $K_2Mo_2O_7$ crystalline domains that are observed to be present on this sample.

It cannot be expected that information regarding the coordination of MoO_x species obtained from ESR data on Mo(V) centers corresponds to the vast majority of Mo(VI) present in the fully oxidized catalysts. However, we have found some important characteristics that can be related to changes that may occur to the Mo(VI)O_x domains with the addition of alkali. It has been stated that surface MoO_x species, when supported on silica, are highly distorted hexacoordinate species irrespective of the preparation method.[44] ESR data indicate that over the Si/Ti 1:1 support this structural distortion is maximized at the alkali level of K/Mo = 0.07. This distortion could be the result of an increased number of Si−O^- ligands attached to the MoO_x-supported species, as would be in agreement with the NMR and DRIFTS results.

Propane ODH Reaction Performance. (K/Mo)/Si−Ti 1:1 catalysts were compared in the propane ODH reaction using equal surface-area loading (65 m^2) in the reactor at a temperature of 550 °C. The feed percentages for these experiments were $N_2/C_3/O_2$ 61:26:13. Reaction data were taken after the steady state was reached. The variation of propylene formation rate with K/Mo ratio for these equal surface-area tests is presented in Figure 20. The propylene formation rate reported here is the "observed" rate that results from the formation and further reaction of propylene. The rate is seen to increase slowly through a maximum between K/Mo = 0.07 and 0.14 and then fall as K/Mo is increased to 0.3 and 0.6, respectively. In previous studies,[31, 70] it has been found that alkaline promoters decrease the acidity and increase the basicity of MoO_x catalysts, this effect

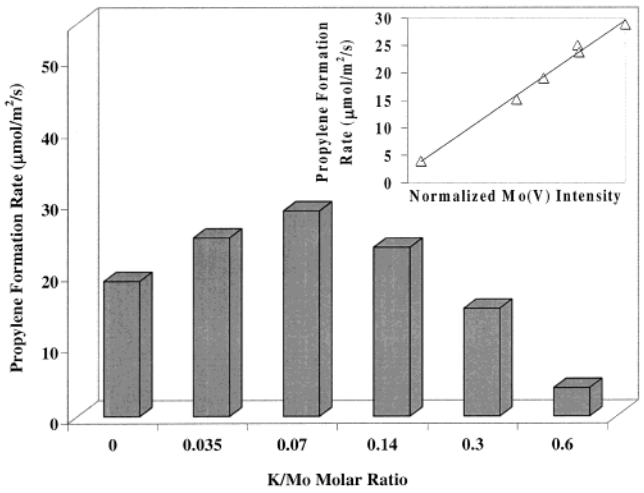

Figure 20. Formation (Δpropylene) rate for equal surface-area (~65 m^2) reaction experiments (μmol/m^2/s). Inset: Propylene formation rate vs Mo(V) ESR intensity (dehydrated conditions).

being maximized at low alkali/Mo ratios. Consequently, the alkali can "weaken" the adsorption of formed propylene, thus facilitating its desorption as a product. Furthermore, it is likely that, when MoO_x domains are supported on a binary oxide, favorable interaction of MoO_x domains with the Si/Ti support can increase not only reactivity but also the accessibility of surface-supported domains. This behavior helps to explain the initial increase of the propylene formation rate during propane ODH at the level of alkali promotion where the favorable support interaction was found to exist.

It is interesting that a linear relationship is obtained when the propylene formation rate is plotted versus the Mo(V) signal intensity obtained in ESR experiments under dehydrated conditions (inset of Figure 20). MoO_x-based catalysts are often believed to operate effectively under reduced conditions where the presence of Mo(V) is essential.[10, 72] Furthermore, it has been claimed that Mo(V) is the active site in propane ODH and other oxidation reactions over MoO_x-based catalsyts.[30,71−74] Whereas Mo(V) is, in all probability, related to the active sites of MoO_x catalysts, it seems more likely that the electronic structure of MoO_x domains (explicitly, the nature of the oxygen atoms) is the underlying factor in determining the "activity" over the Mo/Si−Ti 1:1 catalysts. This electronic structure may also be a key factor that influences the MoO_x domain interaction with the binary oxide support.

Structural Changes with the Addition of K. Several studies over MoO_3/SiO_2 catalysts have suggested the specificity of Mo═O bonds for the partial oxidation of methane to formaldehyde whereas Mo−O−Mo bonds contribute to the total oxidation products.[75−77] However, other studies have proposed that Mo═O bonds do not play a critical role in partial oxidation reactions and that it is the nature of the Mo−O−Mo bonds that determines reactivity.[74] It is understood that the oxygen environment around molybdenum is the decisive factor for oxidation reactions. It has been reported that the addition of K to Mo-based catalysts can affect this oxygen environment by causing the cleavage of Mo−O−Mo bonds.[74] Kantschewa et al.[78] have found that over Ni−Mo/Al_2O_3 catalysts the addition of potassium brings about a decrease in reducibility and transforms the coordination of Mo^{6+} from octahedral to tetrahedral at high alkali content. However, surface polymolybdate domains were eliminated, even before any evidence of K−molybdate formation was observed. This phenomenon was accompanied by the stabilization of Mo in the +5 oxidation state. It has also been reported that below the level where new compounds are formed the addition of alkali can significantly reduce the Lewis acidity of Mo(VI) ions without drastically changing the structure.[31,79] Poor dispersion of MoO_x over silica is usually ascribed to the low reactivity of surface silanols. However, results presented here indicate that MoO_x surface species interact with both silica and titania domains of the support. Furthermore, with the addition of low levels of potassium, distorted MoO_x units experiencing decreased Lewis acidity could be more reactive toward electronegative $Si-O^-$ support ligands on the Si/Ti 1:1 support, which helps to explain the concurrent trend of the ESR results on the coordination of Mo(V) species with that of the decrease in available free hydroxyls obtained in the NMR and DRIFTS experiments.

The ESR results presented herein do not indicate a loss of oxygen but rather significant electronic interaction of K with the MoO_x domains. This interaction could be strong enough to "force" MoO_x domains to interact with silica by forming more Mo−O−Si bonds. Although the exact nature of this interaction has not been determined, a highly distorted structure sharing both titania and silica ligands may account for the observed increase in reactivity at the low K/Mo molar ratios. Raman data suggest that the best dispersion over the Si/Ti 1:1 support is obtained before the onset of K−molybdate formation. Furthermore, analysis of the bulk structure, which shows continuous segregation of titania as anatase crystallites, shows that the best MoO_x dispersion may be obtained over a support where titania remains as nanodispersed TiO_x regions.

Conclusions

The Si/Ti 1:1 mixed oxide support is in a state of nanodispersed titania (anatase) over silica. With the introduction of molybdenum and successive levels of alkali promoter, the dispersion of titania decreases, as does the interaction of TiO_x species with silica. Concurrent with this change is the observation of an enhanced interaction of the MoO_x species with silica. Raman spectroscopy suggests that low levels of alkali (K/Mo = 0.035−0.14) promote the formation of more isolated surface species interacting with silica, whereas higher alkali content leads to the formation of K−molybdate species. In agreement with these results is the fact that the silica network of the support experiences a loss in free hydroxyls at the same level of alkali.

The presence of potassium significantly alters the electronic structure of the surface MoO_x domains, even before the onset of K−molybdate formation. This electronic interaction is observed readily in the ESR spectrum of dehydrated samples. Data suggest that surface-supported species, present as distorted octahedral MoO_x, become the most distorted at low levels of alkali (K/Mo = 0.07). When tested in propane ODH, the activity shows an initial increase at the same low alkali content followed by a sharper decline. A linear relationship is obtained when the propylene formation rate is plotted versus the Mo(V) signal intensity obtained in ESR experiments for the K/Mo/Si−Ti 1:1 catalysts. Although Mo(V) is not specifically assigned as the active site of propane ODH, the concentration of Mo(V)is indicative of the electronic interaction of K resulting in the observed structural effects on the oxygen environment of MoO_x domains. It was found that with the addition of low levels of potassium distorted MoO_x units, experiencing decreased Lewis acidity, could to be more reactive toward electronegative $Si-O^-$ support ligands on the Si/Ti 1:1 support. Although the exact structure of this interaction species has not been determined, a highly distorted structure sharing both titania and silica ligands may be linked to the observed increase in propane ODH reactivity at the low K/Mo molar ratios.

Acknowledgment. Financial support provided by the National Science Foundation (grant no. CTS-9412544) is gratefully acknowledged.

References and Notes

(1) Kung, H. H. *Adv. Catal.* **1994**, *40*, 1.
(2) Mamedov, E. A.; Cortés Corberán, V. *Appl. Catal., A* **1995**, *127*, 1.
(3) Cavani, F.; Trifiro, F. *Catal. Today* **1995**, *24*, 307.
(4) Blasko, T.; López Nieto, J. M. *Appl. Catal., A* **1997**, *157*, 117.
(5) Baerns, M.; Buyevskaya, O. *Catal. Today* **1998**, *45*, 13.
(6) Chen, K.; Khodakov, A.; Yang, J.; Bell, A. T.; Iglesia, E. *J. Catal.* **1999**, *186*, 325.
(7) Khodakov, A.; Olthof, B.; Bell, A. T.; Iglesia, E. *J. Catal.* **1999**, *181*, 205.
(8) Chen, K.; Xie, S.; Iglesia, E.; Bell, A. T. *J. Catal.* **2000**, *189*, 421.
(9) Chen, K.; Xie, S.; Iglesia, E.; Bell, A. T. *J. Catal.* **2000**, *198*, 232.
(10) Schlogl, R.; Knop-Gericke, A.; Hävecker, M.; Wild, U.; Frickel, D.; Ressler, T.; Jentoft, R. E.; Wienold, J.; Mestl, G.; Blume, A.; Timpe, O.; Uchida, Y. *Top. Catal.* **2001**, *15*, 219.
(11) Rajagopal, S.; Grimm, T. L.; Collins, D. J.; Miranda, R. *J. Catal.* **1992**, *137*, 453.
(12) Damyanova, S.; Spojakina, A.; Jiratova, K. *Appl. Catal., A* **1995**, *125*, 257.
(13) Reddy, B. M.; Chowdhury, B.; Smirniotis, P. G. *Appl. Catal., A* **2001**, *211*, 19.
(14) Mori, K.; Inomata, M.; Miyamoto, A.; Murakami, Y. *J. Phys. Chem.* **1983**, *87*, 4560.
(15) Lopez Nieto, J. M.; Kremenic, G.; Fierro, J. L. G. *Appl. Catal., A* **1990**, *61*, 235.
(16) Quaranta, N. E.; Soria, J.; Cortes Corberan, V.; Fierro, J. L. G. *J. Catal.* **1997**, *171*, 1.
(17) Reiche, M. A.; Ortelli, E.; Baiker, A. *Appl Catal., B* **1999**, *23*, 187.
(18) Notari, B. *Adv. Catal.* **1994**, *41*, 253.
(19) Gao, X.; Wachs, I. E. *Catal. Today* **1999**, *51*, 233.
(20) Gao, X.; Bare, S. R.; Fierro, J. L. G.; Banarez, M. J.; Wachs, I. E. *J. Phys. Chem.* **1998**, *102*, 5653.
(21) Ko, E. I.; Chen, J.-P.; Weissman, J. G. *J. Catal.* **1987**, *105*, 511.
(22) Kumbhar, P. S. *Appl. Catal.* **1993**, *96*, 241.
(23) Baiker, A.; Dollenmeier, P.; Glinski, M. *Appl. Catal., A* **1987**, *35*, 365.
(24) Gao, X.; Bare, S. R.; Fierro, J. L. G.; Wachs, I. E. *J. Phys. Chem.* **1999**, *103*, 618.
(25) Gao, X.; Wachs, I. E. *J. Catal.* **2000**, *192*, 18.
(26) Chen, K.; Bell, A. T.; Iglesia, E. *J. Phys. Chem.* **2000**, *104*, 1292.
(27) Akimoto, M.; Echigoya, E. *J. Catal.* **1974**, *35*, 278.
(28) Mross, W. D. *Catal. Rev.—Sci. Eng.* **1983**, *25*, 591.
(29) Erdohelyi, A.; Mate, F.; Solymosi, F. *J. Catal.* **1992**, *135*, 563.
(30) Abello, M. C.; Gomez, M. F.; Cadus, L. E. *Catal. Lett.* **1998**, *53*, 185.
(31) Watson, R. B.; Ozkan, U. S. *J. Catal.* **2000**, *191*, 12.
(32) Izutsu, H.; Nair, P. K.; Maeda, K.; Kiyozumi, Y.; Mizukami, F. *Mater. Res. Bull.* **1997**, *32*, 1303.
(33) Cullity, B. D. In *Elements of X-ray Diffraction*; Cohen M., Ed.; Addison-Wesley: Redding, MA, 1978.
(34) Brinker, C. J.; Scherer, D. W. *Sol−Gel Science: The Physics and Chemistry of Sol−Gel Processing*; Academic Press: Boston, 1990.
(35) Del Arco, M.; Sanfelipe, M. F. M.; Rives, V.; Malet, P.; Ulibarri, M. A. *J. Mater. Sci.* **1992**, *27*, 2960.
(36) Fernandez, A.; Leyrer, J.; Gonzalez-Elipe, A. R.; Munuera, G.; Knozinger, H. *J. Catal.* **1988**, *112*, 489.
(37) Notari, B. *Adv. Catal.* **1994**, *41*, 253.
(38) Dirken, P. J.; Smith, M. E.; Whitfield, H. J. *J. Phys. Chem.* **1995**, *99*, 395.
(39) Stakheev, A. Y.; Shpiro, E. S.; Apijok, J. *J. Phys. Chem.* **1993**, *97*, 5668.
(40) Watson, R. B.; Ozkan, U. S. Mo Loading Effects Over Mo/Si/Ti Catalysts in the Oxidative Dehydrogenation of Ethane. *J. Catal.*, in press.
(41) Gao, X.; Bare, S. R.; Fierro, J. L. G.; Weckhuysen, B. M.; Wachs, I. E. *J. Phys. Chem. B* **1998**, *102*, 10842.
(42) Armaroli, T.; Milella, F.; Notari, B.; Willey, R. J.; Busca, G. *Top. Catal.* **2001**, *15*, 63.
(43) Izutsu, H.; Nair, P. K.; Maeda, K.; Kiyozumi, Y.; Mizukami, F. *Mater. Res. Bull.* **1997**, *32*, 1303.
(44) Banares, M. A.; Hu, H.; Wachs, I. E. *J. Catal.* **1994**, *150*, 407.
(45) Williams, C. C.; Ekerdt, J. G.; Jehng, J. M.; Hardcastle, F. D.; Turek, A. M.; Wachs, I. E. *J. Phys. Chem.* **1991**, *95*, 8781.
(46) Weckhuysen, B. M.; Jehng, J. M.; Wachs, I. E. *J. Phys. Chem.* **2000**, *104*, 7382.
(47) Erdohelyi, A.; Fodor, K.; Solymosi, F. *J. Catal.* **1997**, *166*, 244.
(48) Takenaka, S.; Tanaka, T.; Funabiki, T.; Yoshida, S. *J. Phys. Chem.* **1998**, *102*, 2960.
(49) Wachs, I. E. *Catal. Today* **1996**, *27*, 437.
(50) Chen, K.; Xie, S.; Bell, A. T.; Iglesia, E. *J. Catal.* **2000**, *195*, 244.
(51) Banares, M. A.; Spencer, N. D.; Jones, M. D.; Wachs, I. E. *J. Catal.* **1994**, *144*, 204.
(52) Banares, M. A.; Hu, H.; Wachs, I. E. *J. Catal.* **1995**, *155*, 249.
(53) Rodrogo, L.; Marcinkowska, K.; Adnot, A.; Kaliaguine, S.; Stencel, J. M.; Makovsky, L. E.; Diehl, J. R. *J. Phys. Chem.* **1986**, *90*, 2690.
(54) Walther, K. L.; Wokaum, A.; Handy, B. E.; Baiker, A. *J. Non-Cryst. Solids* **1991**, *134*, 47.
(55) Liu, Z.; Crumbaugh, G. M.; Davis, R. J. *J. Catal.* **1996**, *159*, 83.
(56) Davis, R. D.; Liu, Z. *Chem. Mater.* **1997**, *9*, 2311.
(57) Gittleman, C. S.; Watanabe, K.; Bell, A. T.; Radke, C. J. *Microporous Mater.* **1996**, *6*, 131.
(58) Takei, T.; Kato, K.; Meguro, A.; Chikazawa, M. *Colloids Surf., A* **1999**, *150*, 77.
(59) Little, L. H. *Infrared Spectra of Adsorbed Species*; Academic Press: New York, 1966.
(60) Chary, K. V. R.; Vijayakumar, V.; Rao, P. K.; Nosov, A. V.; Mastikhin, V. M. *J. Mol. Catal.* **1995**, *96*, L5.
(61) Sojka, Z.; Che, M. *Surf. Chem. Catal.* **2000**, *3*, 163.
(62) Cadus, L. E.; Abello, M. C.; Gomez, M. F.; Rivarola, J. B. *Ind. Eng. Chem. Res.* **1996**, *35*, 14.
(63) Xhao, Q.; Bao, X.; Wang, Y.; Lin, L.; Li, G.; Guo, X.; Wang, X. *J. Mol. Catal.* **2000**, *157*, 265.
(64) Kucherov, A. V.; Kucherova, T. N.; Slinkin, A. A. *Micropor. Mater.* **1998**, *26*, 1.
(65) Kucherov, A. V.; Slinkin, A. A. *Catal. Lett.* **2000**, *64*, 53.
(66) Boudlich, D.; Haddad, M.; Nadiri, A.; Berger, R.; Kliava, J. *J. Non-Cryst. Solids* **1998**, *224*, 135.
(67) Sojka, Z.; Adamski, A.; Che, M. *J. Mol. Catal.* **1996**, *112*, 469.
(68) Louis, C.; Che, M.; Anpo, M. *J. Catal.* **1993**, *141*, 453.
(69) Che, M.; Sojka, Z. *Top. Catal.* **2001**, *15*, 2.
(70) Grabowski, R.; Grzybowska, B.; Samson, K.; Sloczynski, J.; Stoch, J.; Wcislo, K. *Appl. Catal.* **1995**, *125*, 129.
(71) Zhang, B.; Liu, N.; Lin, Q.; Jin, D. *J. Mol. Catal.* **1991**, *65*, 15.
(72) Cadus, L. E.; Abello, M. C.; Gomez, M. F.; Rivarola, J. B. *Ind. Eng. Chem. Res.* **1996**, *35*, 14.
(73) Cadus, L. E.; Gomez, M. F.; Abello, M. C. *Catal. Lett.* **1997**, *43*, 229.
(74) Banares, M. *Catal. Today* **1999**, *51*, 319.
(75) de Lucas, A.; Valverde, J. L.; Rodriguez, L.; Sanchez, P.; Garcia, M. T. *Appl. Catal.* **2000**, *203*, 81.
(76) Smith, M.; Ozkan, U. *J. Catal.* **1993**, *142*, 226.
(77) Arena, F.; Giordano, N.; Parmiliana, A. *J. Catal.* **1997**, *167*, 269.
(78) Kantschewa, M.; Delannay, F.; Jeziorowski, H.; Delgado, E.; Eder, S.; Ertl, G.; Knozinger, H. *Appl. Catal.* **1983**, *8*, 71.
(79) Chen, K.; Xie, S.; Bell, A. T.; Iglesia, E. *J. Catal.* **2000**, *195*, 244.